Chapter 9
Transition to Absolute Instability in Porous Media: Numerical Solutions

9.1 A Variant Prats Problem with Uniform Heat Flux

Let us consider a horizontal porous channel having a rectangular cross section with height L. We adopt a two-dimensional description where the coordinates are chosen so that x is the longitudinal horizontal axis and z is the transverse vertical axis. We are assuming heating from below with a uniform heat flux, q_0, at $z = 0$, while the upper boundary, $z = L$, is kept isothermal with temperature T_2. We point out that this setup is just the same considered in Sect. 7.7 as a possible variant of the Horton–Rogers–Lapwood problem. By analogy with the Prats problem [4], the presence of a horizontal flow along the x-direction is taken into account.

9.1.1 Dimensionless Formulation

The velocity field, $\mathbf{u} = (u, w)$, and the temperature field, T, as well as the coordinates, (x, z), and time, t, can be written in a dimensionless form by adopting the transformation

$$(u, w)\,\frac{L}{\alpha} \to (u, w)\ , \qquad (T - T_2)\,\frac{\varkappa_{\text{eff}}}{q_0 L} \to T\ ,$$

$$(x, z)\,\frac{1}{L} \to (x, z)\ , \qquad \frac{t}{L^2/\alpha} \to t\ , \tag{9.1}$$

where α is the average thermal diffusivity and $\varkappa_{\text{eff}}$ is the average thermal conductivity of the porous medium. Through this scaling, the Oberbeck–Boussinesq approximation of the governing local balance equations is still given by Eq. (8.2), where the Darcy–Rayleigh number is now defined as

A. Barletta, *Routes to Absolute Instability in Porous Media*,
https://doi.org/10.1007/978-3-030-06194-4_9

$$R = \frac{g\,\beta\,q_0\,K\,L^2}{\nu\,\alpha\,\varkappa_{\rm eff}}\ , \tag{9.2}$$

while the boundary conditions are expressed as

$$\begin{aligned} z = 0\ :\quad & w = 0\ , \quad \frac{\partial T}{\partial z} = -1\ , \\ z = 1\ :\quad & w = 0\ , \quad T = 0\ . \end{aligned} \tag{9.3}$$

By analogy with what we did for the analysis of the Prats problem carried out in Chap. 8, we introduce a streamfunction ψ, defined as

$$u = \frac{\partial \psi}{\partial z}\ , \qquad w = -\,\frac{\partial \psi}{\partial x}\ , \tag{9.4}$$

so that the governing local balance equations are now formulated as

$$\begin{aligned} & \frac{\partial^2 \psi}{\partial x^2} + \frac{\partial^2 \psi}{\partial z^2} + R\,\frac{\partial T}{\partial x} = 0\ , \\ & \sigma\,\frac{\partial T}{\partial t} + \frac{\partial \psi}{\partial z}\,\frac{\partial T}{\partial x} - \frac{\partial \psi}{\partial x}\,\frac{\partial T}{\partial z} = \frac{\partial^2 T}{\partial x^2} + \frac{\partial^2 T}{\partial z^2}\ . \end{aligned} \tag{9.5}$$

With this formulation, we can express the boundary conditions (9.3) as

$$\begin{aligned} z = 0\ :\quad & \frac{\partial \psi}{\partial x} = 0\ , \quad \frac{\partial T}{\partial z} = -1\ , \\ z = 1\ :\quad & \frac{\partial \psi}{\partial x} = 0\ , \quad T = 0\ . \end{aligned} \tag{9.6}$$

The stationary solution, $(\psi_{\rm b}, T_{\rm b})$, of the governing equations (9.5) and boundary conditions (9.6) is still expressed by Eq. (8.8). It describes a uniform velocity in the x-direction, with a vertical temperature gradient,

$$\psi_{\rm b} = Pe\ z\ , \qquad T_{\rm b} = 1 - z\ . \tag{9.7}$$

Here, Pe is the *Péclet number* relative to the basic horizontal and uniform flow in the porous channel, defined by Eq. (8.9).

The next step is, as usual, assuming small amplitude perturbations of the basic stationary flow,

$$\psi = \psi_{\rm b} + \varepsilon\,\Psi\ , \qquad T = T_{\rm b} + \varepsilon\,\Theta\ , \tag{9.8}$$

such that $|\varepsilon| \ll 1$. The linearised equations for the perturbation fields (Ψ, Θ) are solutions of the partial differential equations

$$\frac{\partial^2 \Psi}{\partial x^2} + \frac{\partial^2 \Psi}{\partial z^2} + R\,\frac{\partial \Theta}{\partial x} = 0\,,$$

$$\sigma\,\frac{\partial \Theta}{\partial t} + Pe\,\frac{\partial \Theta}{\partial x} + \frac{\partial \Psi}{\partial x} = \frac{\partial^2 \Theta}{\partial x^2} + \frac{\partial^2 \Theta}{\partial z^2}\,, \tag{9.9}$$

with the boundary conditions

$$z = 0\ :\quad \frac{\partial \Psi}{\partial x} = 0\,,\quad \frac{\partial \Theta}{\partial z} = 0\,,$$

$$z = 1\ :\quad \frac{\partial \Psi}{\partial x} = 0\,,\quad \Theta = 0\,. \tag{9.10}$$

We express the perturbations, (Ψ, Θ), through their Fourier transforms, $(\tilde{\Psi}, \tilde{\Theta})$, as exploited in Eq. (8.13), and we write

$$\tilde{\Psi} = f(z)\,\mathrm{e}^{\lambda(k)\,t}\,,\qquad \tilde{\Theta} = -\,\mathrm{i}\,k\,h(z)\,\mathrm{e}^{\lambda(k)\,t}\,. \tag{9.11}$$

Thus, the differential eigenvalue problem for the stability analysis is obtained from Eqs. (9.9) and (9.10) and reads

$$\left(\frac{\mathrm{d}^2}{\mathrm{d}\,z^2} - k^2\right) f + R\,k^2\,h = 0\,,$$

$$\left[\frac{\mathrm{d}^2}{\mathrm{d}\,z^2} - k^2 - \gamma(k)\right] h + f = 0\,,$$

$$z = 0\ :\quad f = 0\,,\quad \frac{\mathrm{d}\,h}{\mathrm{d}\,z} = 0\,,$$

$$z = 1\ :\quad f = 0\,,\quad h = 0\,, \tag{9.12}$$

where

$$\gamma(k) = \sigma\,\lambda(k) + \mathrm{i}\,k\,Pe\,. \tag{9.13}$$

Due to the boundary conditions prescribed for the eigenfunctions $(f\,, h)$, it is impossible to express the solution of Eq. (9.12) in terms of a simple sine function, as in the classical formulation of Prats problem with impermeable isothermal boundaries. In fact, a sine function, $\sin(n\,\pi\,z)$, fulfils the boundary conditions for f, but not those for h. Obviously, Eq. (9.12) can be solved analytically by employing the characteristic equation method, but this approach leads to an implicit dispersion relation, as described in Sect. 7.7.2. Then, there is no great advantage in tackling the stability analysis with this technique. A numerical solution is preferable.

Our focus is not a dispersion relation in the classical sense, but its differential counterpart, namely the eigenvalue problem (9.12).

9.1.2 Convective Instability

The convective instability analysis starts from the principle of exchange of stabilities. One can employ just the same reasoning provided in Sect. 7.7.1, the only difference is that γ appears in Eq. (9.12) instead of λ. Thus, we can prove that

$$\Im(\gamma)\, R k^2 \int_0^1 |h|^2 \, \mathrm{d}z = 0 \,, \tag{9.14}$$

by the same arguments employed for the proof of Eq. (7.115). Our conclusion is that $\Im(\gamma) = 0$. Since $\lambda = \eta - \mathrm{i}\,\omega$, on account of Eq. (9.13), we can write

$$\omega = \frac{k\, Pe}{\sigma} \,. \tag{9.15}$$

This is just the same conclusion drawn in Eq. (8.20) relative to the Prats problem with isothermal conditions at both boundaries $z = 0, 1$. It can be rephrased as $\gamma = \sigma\, \eta$. Then, the neutral stability condition ($\eta = 0$) is determined by the numerical solution of Eq. (9.12) with $\gamma = 0$,

$$\begin{gathered}
\left(\frac{\mathrm{d}^2}{\mathrm{d}\, z^2} - k^2\right) f + R k^2 h = 0 \,, \\
\left(\frac{\mathrm{d}^2}{\mathrm{d}\, z^2} - k^2\right) h + f = 0 \,, \\
z = 0 \,: \quad f = 0 \,, \quad \frac{\mathrm{d}\, h}{\mathrm{d}\, z} = 0 \,, \\
z = 1 \,: \quad f = 0 \,, \quad h = 0 \,.
\end{gathered} \tag{9.16}$$

This finding allows one to establish an important fact. The neutral stability condition, determined by the solution of Eq. (9.16), is independent of the Péclet number, Pe. Thus, one can determine such condition for the case $Pe = 0$. This special case is that examined in Sect. 7.7.2. In other words, the neutral stability curve, evaluated numerically, is that drawn in Fig. 7.11. The solution of Eq. (9.16) is employed to determine the numerical function $R(k)$, i.e. the neutral stability function. In other words, R is computed as the eigenvalue of Eq. (9.16), for every prescribed value of $k \in \mathbb{R}$. The result of this computation is provided in Fig. 7.11. This figure shows the point of minimum R along the neutral stability curve, i.e. the critical point for convective instability. The critical values of the wave number and of the Darcy–Rayleigh number are, in fact,

$$k_c = 2.32621 \,, \qquad R_c = 27.0976 \,. \tag{9.17}$$

Such behaviour is qualitatively the same found for the Prats problem with isothermal boundaries, studied in Sect. 8.2.3. The neutral stability condition is not affected by the basic horizontal flow, and the neutral stability curve is thus the same as for the case $Pe = 0$, namely for the limiting case where the Prats problem coincides with the Horton–Rogers–Lapwood problem.

9.1.3 Absolute Instability

The study of absolute instability relies on the steepest-descent approximation of the perturbation wave packets,

$$\Psi(x, z, t) = \frac{1}{\sqrt{2\pi}} \int_{-\infty}^{\infty} \mathrm{e}^{\lambda(k)\, t + \mathrm{i}\, k\, x} f(z)\, \mathrm{d}\, k \,,$$

$$\Theta(x, z, t) = -\frac{\mathrm{i}}{\sqrt{2\pi}} \int_{-\infty}^{\infty} k\, \mathrm{e}^{\lambda(k)\, t + \mathrm{i}\, k\, x} h(z)\, \mathrm{d}\, k \,. \tag{9.18}$$

Hence, the first step is the determination of the saddle points in the complex plane, $k = k_0 \in \mathbb{C}$, such that $\lambda'(k) = 0$. The threshold of absolute instability occurs when the prescribed value of R detects the condition of zero asymptotic growth, $\Re(\lambda(k_0)) = 0$. This threshold condition defines R_a.

The basis for the evaluation of R_a is still the eigenvalue problem (9.12), together with Eq. (9.13). However, the numerical solution of Eq. (9.12) must be approached with the specification that $k = k_r + \mathrm{i}\, k_i$ is a complex variable with real part k_r and imaginary part k_i. We assume Pe and R to be prescribed quantities. The fulfilment of the saddle-point condition can be automatically implemented by forcing the constraint $\lambda'(k) = 0$. One can implement this constraint by doubling the order of the differential problem (9.12). To this end, we define

$$\hat{f} = \frac{\partial f}{\partial k} \,, \qquad \hat{h} = \frac{\partial h}{\partial k} \,. \tag{9.19}$$

Then, we obtain the extended eigenvalue problem

$$\frac{\mathrm{d}^2 f}{\mathrm{d}\, z^2} - k^2 f + R\, k^2\, h = 0 \,,$$

$$\frac{\mathrm{d}^2 h}{\mathrm{d}\, z^2} - \left[k^2 + \sigma\, \lambda(k) + \mathrm{i}\, k\, Pe\right] h + f = 0 \,,$$

$$\frac{\mathrm{d}^2\hat{f}}{\mathrm{d}\,z^2} - k^2\,\hat{f} + R\,k^2\,\hat{h} - 2\,k\,f + 2\,R\,k\,h = 0\,,$$

$$\frac{\mathrm{d}^2\hat{h}}{\mathrm{d}\,z^2} - \left[k^2 + \sigma\,\lambda(k) + \mathrm{i}\,k\,Pe\right]\hat{h} + \hat{f} - (2\,k + \mathrm{i}\,Pe)\,h = 0\,,$$

$$z = 0\ :\quad f = 0\,,\quad \frac{\mathrm{d}\,h}{\mathrm{d}\,z} = 0\,,\quad \hat{f} = 0\,,\quad \frac{\mathrm{d}\,\hat{h}}{\mathrm{d}\,z} = 0\,,$$

$$z = 1\ :\quad f = 0\,,\quad h = 0\,,\quad \hat{f} = 0\,,\quad \hat{h} = 0\,, \tag{9.20}$$

where we took into account that $\gamma(k) = \sigma\,\lambda(k) + \mathrm{i}\,k\,Pe$ and that $\lambda'(k) = 0$. The notation seems a bit equivocal as, on writing Eq. (9.19), we intend $(f\,,h)$ as functions of k and z, while the extended eigenvalue problem is written by employing the symbol of ordinary derivatives with respect z, that is $\mathrm{d}/\mathrm{d}z$. This choice is made for internal consistency with the convention applied so far in this book, and because there are not reasonable possibilities to mistake the meaning of this notation. We finally note that there is no ambiguity as Eq. (9.20) involves only ordinary differential equations, as the only derivatives employed there are derivatives with respect to z.

The solution of Eq. (9.20) can be worked out by assuming an eigenvalue problem structure. In this sense, there is no formal difference with respect to the solution of Eq. (9.16). In the case of problem (9.20), the procedure is more complicated because the eigenfunctions are four, $(f\,,h,\hat{f}\,,\hat{h})$, instead of two, as in Eq. (9.16). Moreover, $(f\,,h,\hat{f}\,,\hat{h})$ are complex-valued, while the eigenfunctions $(f\,,h)$ of problem (9.16) are real-valued. These facts do not alter the intrinsic nature of Eq. (9.20), which is the same as that of Eq. (9.16). They are both ordinary differential eigenvalue problems. This means that the numerical technique for their solution is, in principle, just the same. For details, we refer the reader to Chap. 10, while for alternatives such as the compound matrix method or the Chebyshev tau method we mention the papers by Straughan and Walker [5] and by Dongarra et al. [2].

The strategy in the solution of Eq. (9.20) is based on the general characteristics of the saddle points $k_0 \in \mathbb{C}$ pertinent for the determination of the threshold value $R = R_\mathrm{a}$ for the transition from convective to absolute instability. These characteristics are the fulfilment of

$$\lambda'(k) = 0\,, \tag{9.21}$$

which is a built-in feature of the eigenvalue problem (9.20), and the requirement

$$\Re(\lambda(k)) = 0\,. \tag{9.22}$$

This requirement must be considered as an input datum, inasmuch as the value of Pe. The output constants to be determined, namely the eigenvalues, are

$$\Re(k)\,,\quad \Im(k)\,,\quad \Im(\sigma\,\lambda(k))\,,\quad R\,. \tag{9.23}$$

In order to check if this solution strategy is consistent, we reformulate Eq. (9.20) as an initial value problem, by introducing suitably defined unknown constants. We expand the conditions at the lower boundary so that now we have

$$z = 0 \; : \quad f = 0 \,, \quad \frac{\mathrm{d}f}{\mathrm{d}z} = 1 \,, \quad h = a_1 \,, \quad \frac{\mathrm{d}h}{\mathrm{d}z} = 0 \,,$$

$$\hat{f} = 0 \,, \quad \frac{\mathrm{d}\hat{f}}{\mathrm{d}z} = 0 \,, \quad \hat{h} = a_2 \,, \quad \frac{\mathrm{d}\hat{h}}{\mathrm{d}z} = 0 \,. \tag{9.24}$$

Setting $\mathrm{d}f/\mathrm{d}z = 1$ serves only to fix the, otherwise arbitrary, scale of the eigenfunctions $(f, h, \hat{f}, \hat{h})$. The condition $\mathrm{d}\hat{f}/\mathrm{d}z = 0$ is a consequence of this scale-fixing constraint. It is obtained from $\mathrm{d}f/\mathrm{d}z = 1$ by taking its derivative with respect to k and by employing Eq. (9.19). The complex constants a_1 and a_2 must be determined, together with the real variables listed in Eq. (9.23), by imposing the end conditions at the upper boundary,

$$z = 1 \; : \quad f = 0 \,, \quad h = 0 \,, \quad \hat{f} = 0 \,, \quad \hat{h} = 0 \,. \tag{9.25}$$

The end conditions are relative to complex eigenfunctions. Thus, they effectively correspond to eight real equations. They are enough to determine the four real variables given by Eq. (9.23) and the four real variables given by the real and imaginary parts of a_1 and a_2. We point out that the complex constants a_1 and a_2 are internal variables with no direct physical meaning. In fact, their values are a consequence of the condition $\mathrm{d}f/\mathrm{d}z = 1$ imposed to fix, in an arbitrary manner, the scale of the eigenfunctions. A change in this scale-fixing condition alters the values of a_1 and a_2, while it does not modify the values of the four real variables listed in Eq. (9.23).

We refer the reader to Chap. 10 for a more detailed description of the numerical algorithms employed and of their implementation. The framework for the evaluation of the variables given by Eq. (9.23) is, in fact, the shooting method. Its use is based on a root-finding technique in order to impose the end conditions (9.25). Finding numerically the roots of Eq. (9.25) is possible if one suitably initialises the procedure by prescribing guess values of the unknown variables to be determined. The efficient way to achieve this task is starting from a parametric condition where the solution is known, and then incrementing step by step the input value of Pe by small amounts, in order to track the change of the solution with the Péclet number. The guess values at a given step are the computed eigenvalues at the previous step. The smaller is the step, i.e. the smaller is the amount of the Pe increment, the better is the choice of the guess values.

In fact, a case where the value of R_a for a given Pe can be easily guessed is $Pe = 0$. In this case, one expects $R_\mathrm{a} = R_\mathrm{c} = 27.0976$. Consistently, in this case, one expects also

$$\Re(k_0) = \pm k_\mathrm{c} = \pm 2.32621 \,, \quad \Im(k_0) = 0 \,, \quad \Im(\sigma\,\lambda(k_0)) = 0 \,. \tag{9.26}$$

These predictions are grounded on the idea that the rest state ($Pe = 0$) is one where there is no parametric gap between convective and absolute instabilities, namely $R_a = R_c$. In fact, when there is no basic flow driving the perturbation downstream, the Fourier normal modes are non-travelling, so that they amplify or damp in place. This is a consequence of the principle of exchange of stabilities. In such situations, even a single Fourier mode which undergoes an exponential amplification is sufficient to induce an unbounded amplification, for large times, of the whole perturbation wave packet. Beyond this heuristic argument, the principle of exchange of stabilities ensures that, with $Pe = 0$, the critical values $k = \pm k_c$ and $R = R_c$ are the saddle points and their relative Darcy–Rayleigh number, R, yielding the threshold to absolute instability. In fact, the principle of exchange of stabilities proved in Sect. 7.7.1, namely for the case $Pe = 0$, ensures that $\Im(\lambda(k)) = 0$, while the condition of neutral stability provides the constraint $\Re(\lambda(k)) = 0$. Therefore, the neutral stability condition implies $\lambda(k) = 0$ and, hence, also $\lambda'(k) = 0$, which is the saddle point condition. Among the neutrally stable k modes, the critical values are selected because they correspond to the minimum condition $\partial R/\partial k = 0$. The latter condition is implicitly assumed on writing the absolute instability eigenvalue problem (9.20). We finally point out that the critical wave numbers are always two, having the same absolute value, while we generally identify k_c with the positive one. The reason is easily gathered from inspection of the convective instability eigenvalue problem (9.16) where k appears only through its square, k^2.

One can keep track of the gradual displacement of the saddle point starting from the real axis $k_0 = \pm 2.32621$, when $Pe = 0$, to the complex k plane when $Pe > 0$. Figure 9.1 displays the migration of the saddle points in the k plane as Pe increases above 0. This figure reveals that the imaginary part of k continuously decreases

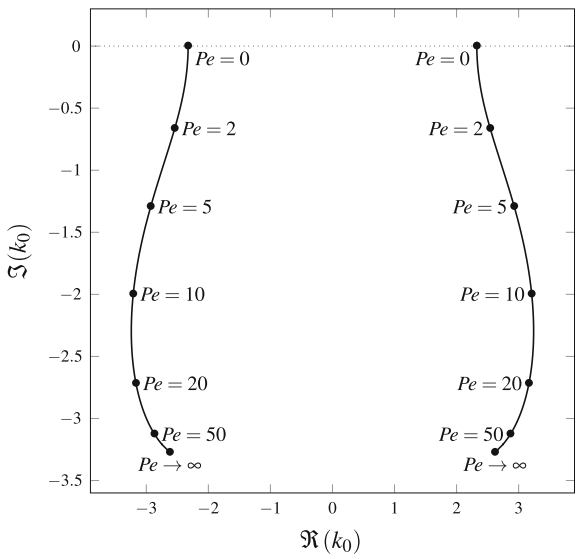

Fig. 9.1 Prats problem with isoflux lower boundary: migration of the pertinent saddle points, with increasing values of Pe, for the threshold to absolute instability

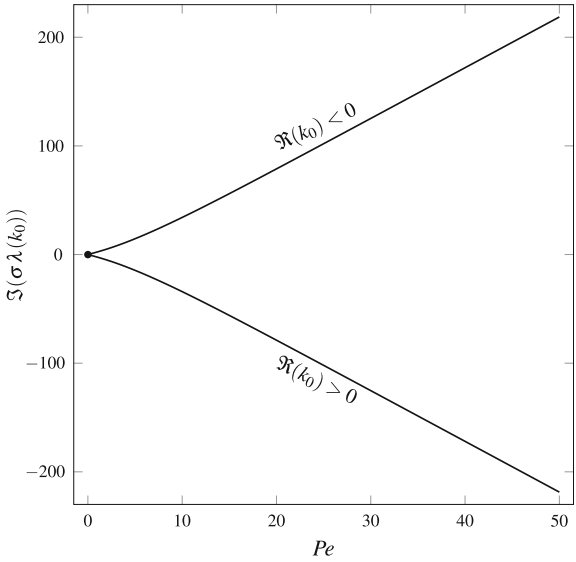

Fig. 9.2 Prats problem with isoflux lower boundary: plot of $\Im(\sigma\,\lambda(k_0))$ versus Pe for the saddle points k_0, at the threshold to absolute instability, with positive or negative $\Re(k_0)$

below 0, while the real part undergoes a non-monotonic trend. Figure 9.1 can be directly compared with Fig. 8.2, relative to the Prats problem with isothermal lower boundary. Figures 8.2 and 9.1 are indeed very similar, especially for large values of Pe. An interesting fact regards the behaviour for the limiting case $Pe \to \infty$. If one considers Eq. (9.20), the asymptotic behaviour for large Péclet numbers can be identified by writing

$$R = \xi\, Pe\ , \quad \sigma\,\lambda = \Lambda\, Pe\ , \quad f = f_{\mathrm{m}}\, Pe\ . \tag{9.27}$$

By substituting Eq. (9.27) into Eq. (9.12), by employing Eq. (9.13) and by keeping the leading terms for large Pe, one obtains

$$h = \frac{f_{\mathrm{m}}}{\Lambda + \mathrm{i}\,k}\ , \tag{9.28}$$

where the modified eigenfunction f_{m} must satisfy the differential equation

$$\left(\frac{\mathrm{d}^2}{\mathrm{d}\,z^2} - k^2 + \frac{\xi\,k^2}{\Lambda + \mathrm{i}\,k}\right) f_{\mathrm{m}} = 0\ , \tag{9.29}$$

with the boundary conditions

$$f_{\mathrm{m}}(0) = 0 = f_{\mathrm{m}}(1)\ . \tag{9.30}$$

Equations (9.29) and (9.30) are solved by writing

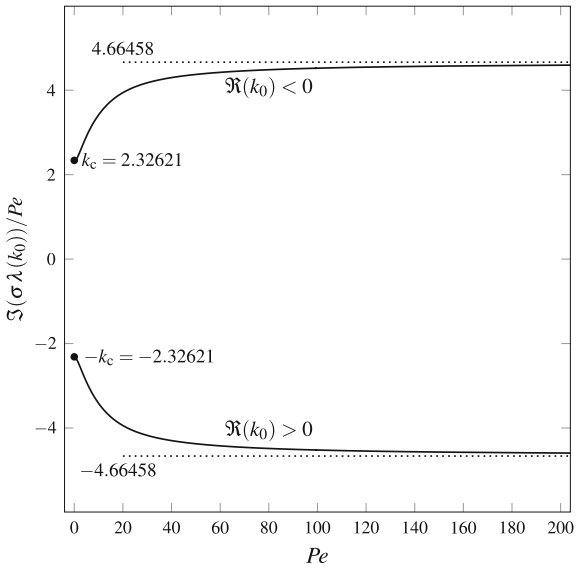

Fig. 9.3 Prats problem with isoflux lower boundary: plot of $\Im(\sigma\ \lambda(k_0)/Pe)$ versus Pe for the saddle points k_0, at the threshold to absolute instability, with positive or negative $\Re(k_0)$. The dotted lines display the asymptotic behaviour given by Eqs. (9.27) and (9.33)

$$f_{\mathrm{m}}(z) = \sin(n\,\pi\,z)\ , \qquad n = 1, 2, 3, \ \ldots\ , \tag{9.31}$$

provided that the dispersion relation

$$\Lambda = \frac{\xi\,k^2}{n^2\pi^2 + k^2} - \mathrm{i}\,k\ , \quad n = 1, 2, 3, \ \ldots \tag{9.32}$$

is satisfied.

Equation (9.32) coincides with Eq. (8.40). This means that the determination of the saddle points and the threshold value of ξ are exactly the same as for the Prats problem with isothermal lower boundary. Hence, the limiting regime $Pe \to \infty$ does not make any difference between the isoflux and isothermal conditions at the lower boundary. One may note that Eq. (9.28) marks an evident incompatibility between the eigenfunction h and the condition of a vanishing derivative $\mathrm{d}h/\mathrm{d}z$ at $z = 0$. This is a consequence of the stretching experienced by the eigenfunctions (f, h) when Pe unboundedly increases. This behaviour results in a singularity as evidenced by Eqs. (9.27) and (9.28). In fact, one can reckon that h becomes negligible with respect to f as $Pe \to \infty$, meaning that either f tends to infinity and h remains finite or f remains finite and h tends to zero. The sensible result is that the saddle points k_0 and the ratio R_{a}/Pe can still be approximated through Eqs. (8.42) and (8.43), if $Pe \gg 1$. In fact, Fig. 9.1 displays also the saddle points k_0 for the limiting case $Pe \to \infty$. As for the parameter Λ introduced in Eq. (9.27), its numerical estimate for $Pe \gg 1$ can be obtained directly from Eq. (9.32), namely

$$k_0 \approx \pm\,2.61941 - \mathrm{i}\,3.27327\ , \quad \Lambda \approx \mp\,\mathrm{i}\,4.66458\ . \tag{9.33}$$

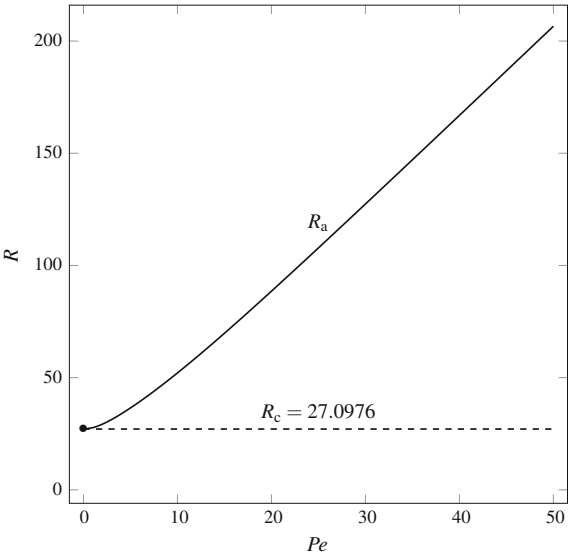

Fig. 9.4 Prats problem with isoflux lower boundary: plot of R_a (solid line) versus Pe, as compared with R_c (dashed line) which is independent of Pe

Equation (9.33) is obtained by substitution of k_0, evaluated for $n = 1$ through Eq. (8.42), as well as of $\xi = R_a/Pe$ given by Eq. (8.43), into Eq. (8.40).

Figure 9.2 shows that the imaginary part of $\sigma\,\lambda(k_0)$ continuously decreases from 0 as Pe increases, for the saddle points with $\Re(k_0) > 0$. The reverse occurs for the twin saddle points having $\Re(k_0) < 0$. The same numerical data over a larger range of Péclet numbers are reported in Fig. 9.3 as plots of $\Im(\sigma\,\lambda(k_0)/Pe)$ versus Pe, in order to illustrate the asymptotic behaviour described by Eqs. (9.27) and (9.33). We note that both $\Im(\sigma\,\lambda(k_0))$ and Pe tend to zero when $Pe \to 0$, while their ratio tends to a finite limit. This finite limiting value can be easily determined on the basis of Eq. (9.15) and on the equalities $k_0 = \pm k_c$, $R_a = R_c$, for $Pe \to 0$. In fact, we reckon that $\Im(\sigma\,\lambda(k_0)/Pe) = \Im(\sigma\,\lambda(\pm k_c)/Pe)$ tends to $\mp k_c = \mp 2.32621$.

The trend of the threshold value R_a for the onset of absolute instability is displayed in Fig. 9.4 as a function of Pe. The critical value R_c is shown for comparison as a dashed line. This figure clearly displays the asymptotic linear trend of R_a versus Pe when $Pe \gg 1$. A neat view of the asymptotic behaviour of R_a/Pe expressed by Eq. (8.43) is shown in Fig. 9.5, where the asymptote, $\xi = R_a/Pe \approx 3.99084$, is drawn as a dotted line. A comparison between Figs. 8.5 and 9.5 is useful. The differences are hardly discernible when $Pe > 10$. This observation is congruent with our previous findings regarding the poor influence on the transition to absolute instability of the thermal boundary condition at the lower boundary, when the horizontal through flow becomes more and more intense.

Figure 9.6 shows the isolines of $\Re(\sigma\,\lambda)$ in the complex k plane for the test case with $Pe = 20$ and $R = R_a = 88.5310$. This map of the lines $\Re(\lambda) = \lambda_r = \text{constant}$ serves as a check of the holomorphy requirement. The paths of steepest descent crossing the saddle points,

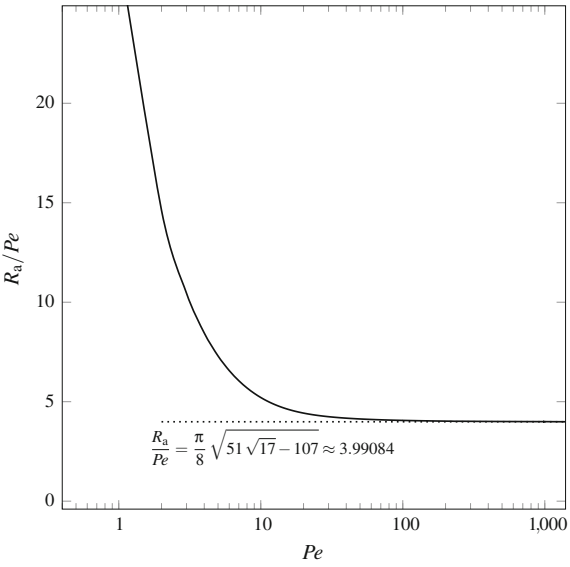

Fig. 9.5 Prats problem with isoflux lower boundary: plot of R_a/Pe (solid line) versus Pe, as compared with its asymptotic value $\xi = R_a/Pe \approx 3.99084$ (dotted line)

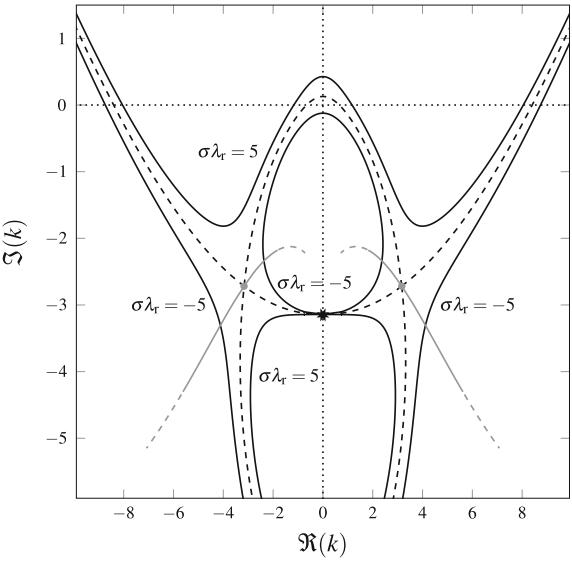

Fig. 9.6 Prats problem with isoflux lower boundary: map of the isolines of $\Re(\lambda) = \lambda_r$ (black solid lines) for $Pe = 20$ and $R = R_a = 88.5310$. The dashed black lines are for $\lambda_r = 0$. The grey dots are the saddle points, while the grey lines are the lines of steepest descent. The black asterisk denotes the singularity $k = -i\,\pi$

$$k_0 = \pm 3.16611 - i\,2.71779\,, \tag{9.34}$$

are drawn in this figure as grey lines. The lines of steepest descent are isolines of $\Im(\lambda)$. In this sample case, they correspond to $\Im(\sigma\,\lambda) = \mp 78.8420$. The map reported in Fig. 9.6 shows that, in fact, there exists a path, locally of steepest descent across the twin saddle points given by Eq. (9.34), that does not trap any singularity of $\Re(\lambda)$

in the region between such path and the real line $\Im(k) = 0$. A singularity is displayed at $k = -\mathrm{i}\,\pi$, thus marking a close analogy to the otherwise only qualitatively similar map reported in Fig. 8.3. The occurrence of such singularity was proved analytically for the Prats problem with isothermal lower boundary, as shown in Sect. 8.2.4. In the case examined in Fig. 9.6, the singularity at $k = -\mathrm{i}\,\pi$ emerges as an upshot of the numerical solution.

9.2 Thermal Instability in a Vertical Porous Channel

Up to this point, we have always investigated cases where the instability was driven by a mechanism of heating from below. However, there are situations such that the instability may occur even in a vertical porous layer, where the basic temperature gradient is the result of side heating.

A fairly simple example was proposed and analysed by Barletta [1]. In this paper, the study is focussed on the convective instability. In Barletta [1], the aim is to show that the classical proof presented by Gill [3] cannot be extended to the case where the porous layer is bounded by permeable planes instead of impermeable walls. The forthcoming analysis involves a situation where, unlike the cases examined by Gill [3] and Barletta [1], a vertical forced flow is present. This variant discloses the possibility of a transition from convective to absolute instability.

9.2.1 Problem Formulation

Let us consider a vertical porous slab bounded by two vertical and permeable planes at $x = \pm L/2$, kept at uniform temperatures T_1 and $T_2 < T_1$, respectively. We note that the generality of our analysis is not influenced in any way by the choice $T_2 < T_1$, as there is no physical difference between the left and right boundaries. On the other hand, when dealing with horizontal layers, it is quite evident that the direction of gravity makes a big physical difference between the lower boundary and the upper boundary.

A sketch of the vertical porous layer, of the coordinate frame and of the boundary conditions is given in Fig. 9.7. The permeable boundaries allow a perfect mechanical and thermal contact with external fluid reservoirs at temperatures T_1 and T_2. Therefore, the boundary pressure at $x = \pm L/2$ is imposed externally. More precisely, we assume that the boundary conditions allow an externally forced pressure gradient, $\partial P/\partial z$, along the vertical z-axis. Such gradient is considered as constant. We recall that P denotes the local difference between the fluid pressure and hydrostatic pressure.

According to all the previous examples, the x and y axes are horizontal with the x-axis perpendicular to the bounding planes, while the z-axis is vertical and upward oriented. We adopt a two-dimensional formulation with all the fields being invariant along the y-direction.

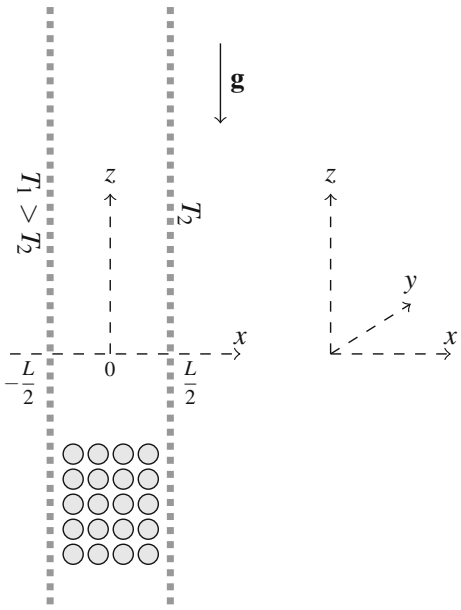

Fig. 9.7 A sketch of the vertical porous layer with permeable boundaries, of the (x, y, z) coordinate frame and of the boundary conditions

We adopt the Oberbeck–Boussinesq approximation and Darcy's law, together with the assumption of a negligible viscous dissipation. Thus, we arrange the dimensionless local balance of mass, momentum and energy in the pressure/temperature formulation according to the two-dimensional version of Eq. (8.79), namely

$$\frac{\partial^2 P}{\partial x^2} + \frac{\partial^2 P}{\partial z^2} - R\,\frac{\partial T}{\partial z} = 0\,,$$

$$\sigma\,\frac{\partial T}{\partial t} - \frac{\partial P}{\partial x}\,\frac{\partial T}{\partial x} - \left[\frac{\partial P}{\partial z} - R\,(T - r)\right]\frac{\partial T}{\partial z} = \frac{\partial^2 T}{\partial x^2} + \frac{\partial^2 T}{\partial z^2}\,, \tag{9.35}$$

where $r = (T_0 - T_2)/(T_1 - T_2)$ is the temperature ratio depending on the choice of the reference temperature, T_0, already introduced in Sect. 8.4, while the dimensionless quantities are scaled as defined by Eqs. (8.1) and (8.80). The Darcy–Rayleigh number, R, is given by Eq. (8.3).

We note that the dimensionless velocity components along the x and z directions are expressed through Darcy's law as

$$u = -\frac{\partial P}{\partial x}\,, \quad w = -\frac{\partial P}{\partial z} + R\,(T - r)\,. \tag{9.36}$$

The boundary conditions are expressed in a dimensionless form as

$$x = -\frac{1}{2}\ : \qquad \frac{\partial P}{\partial z} = -Pe\,, \quad T = 1\,,$$

$$x = \frac{1}{2} \; : \qquad \frac{\partial P}{\partial z} = -Pe \; , \quad T = 0 \; , \tag{9.37}$$

where Pe is the Péclet number associated with the externally forced pressure gradient along the z direction.

9.2.2 The Basic Solution

A stationary solution of Eqs. (9.35) and (9.37) is given by

$$\frac{\partial P_\mathrm{b}}{\partial x} = 0 \; , \quad \frac{\partial P_\mathrm{b}}{\partial z} = -Pe \; , \quad T_\mathrm{b} = \frac{1}{2} - x \; , \tag{9.38}$$

thus describing a vertical flow,

$$u_\mathrm{b} = 0 \; , \quad w_\mathrm{b} = Pe + R \left(\frac{1}{2} - r - x \right) \; , \tag{9.39}$$

where Eqs. (9.36) and (9.38) have been taken into account. The resulting vertical flow is the superposition of an externally forced uniform flow parametrised by the Péclet number, Pe, and a buoyancy-induced flow given by an x dependent linear velocity profile. The latter term depends on both R and r. We note that the net flow rate associated with the basic flow velocity, w_b, is given by

$$\int_{-1/2}^{1/2} w_\mathrm{b} \, \mathrm{d}x = Pe + R \left(\frac{1}{2} - r \right) \; . \tag{9.40}$$

Hence, there is a special value of r such that the buoyant flow term, proportional to R, yields a vanishing contribution to the net flow rate. This special value is $r = (T_0 - T_2)/(T_1 - T_2) = 1/2$ which, in dimensional terms, means a special choice of the reference temperature, i.e. $T_0 = (T_1 + T_2)/2$, the arithmetic mean of the two boundary temperatures, T_1 and T_2.

9.2.3 Stability Analysis

Small perturbations of the basic state (9.39) are defined as

$$P = P_\mathrm{b} + \varepsilon \, \Pi \; , \qquad T = T_\mathrm{b} + \varepsilon \, \Theta \; . \tag{9.41}$$

We substitute Eq. (9.41) into Eqs. (9.35) and (9.37) and neglect terms $O(\varepsilon^2)$. We thus obtain the governing equations for the perturbations,

$$\frac{\partial^2 \Pi}{\partial x^2} + \frac{\partial^2 \Pi}{\partial z^2} - R\,\frac{\partial \Theta}{\partial z} = 0\,,$$

$$\sigma\,\frac{\partial \Theta}{\partial t} + \frac{\partial \Pi}{\partial x} + \left[Pe + R\left(\frac{1}{2} - r - x\right)\right]\frac{\partial \Theta}{\partial z} = \frac{\partial^2 \Theta}{\partial x^2} + \frac{\partial^2 \Theta}{\partial z^2}\,, \tag{9.42}$$

with the boundary conditions

$$x = \pm\frac{1}{2} \;:\quad \frac{\partial \Pi}{\partial z} = 0\,, \quad \Theta = 0\,. \tag{9.43}$$

Equations (9.42) and (9.43) imply that the evolution of perturbations is influenced by the parameter r. This fact marks a deep difference with respect to what happens for the case of a horizontal channel, as pointed out in Sect. 8.4. In other words, for a vertical channel, the choice of the reference temperature T_0 in the formulation of the Oberbeck–Boussinesq approximation matters. One can adopt a twofold approach to this issue:

- Make a mindful choice of T_0 so that the first-order Taylor series expansion of $\rho(T)$, given by Eq. (5.57), is best satisfied. This choice is one where $\rho(T_0)$ is the average density of the fluid or, equivalently, T_0 is the average temperature. Thus, having in mind the base solution (9.38), T_0 is to be chosen as the arithmetic mean of the two boundary temperatures, T_1 and T_2, namely $T_0 = (T_1 + T_2)/2$. This implies that the parameter $r = (T_0 - T_2)/(T_1 - T_2)$ be equal to $1/2$.
- Rescale the Péclet number as

$$Pe^* = Pe + R\left(\frac{1}{2} - r\right)\,. \tag{9.44}$$

  By employing the scaled Péclet number, Pe^*, instead of Pe in Eqs. (9.42) and (9.43), the stability analysis becomes formally independent of r. This option does not imply any specific choice of T_0. On the other hand, this means a redefinition of the Péclet number so that it express the net flow rate along the channel, Pe^*, and not the strength of the vertical pressure gradient, Pe.

Whatever option is chosen, the stability analysis is just the same, being based on the differential problem

$$\frac{\partial^2 \Pi}{\partial x^2} + \frac{\partial^2 \Pi}{\partial z^2} - R\,\frac{\partial \Theta}{\partial z} = 0\,,$$

$$\sigma\,\frac{\partial \Theta}{\partial t} + \frac{\partial \Pi}{\partial x} + (Pe - R\,x)\,\frac{\partial \Theta}{\partial z} = \frac{\partial^2 \Theta}{\partial x^2} + \frac{\partial^2 \Theta}{\partial z^2}\,,$$

$$x = \pm\frac{1}{2} \; : \qquad \frac{\partial \Pi}{\partial z} = 0 \; , \quad \Theta = 0 \; . \tag{9.45}$$

Here, Pe denotes either the Péclet number with $r = 1/2$, or the scaled Péclet number (the asterisk is omitted for simplicity of notation), defined by Eq. (9.44), if we adopt the strategy of not fixing the value of r.

On seeking a solution for Eqs. (9.43) and (9.45) in terms of Fourier transforms, we take into account that the flow direction is the z-axis, so that we define

$$\tilde{\Pi}(k,x,t) = \frac{1}{\sqrt{2\pi}} \int_{-\infty}^{\infty} e^{-\mathrm{i}\,k\,z}\, \Pi(x,z,t)\, \mathrm{d}\,z \; ,$$

$$\Pi(x,z,t) = \frac{1}{\sqrt{2\pi}} \int_{-\infty}^{\infty} e^{\mathrm{i}\,k\,z}\, \tilde{\Pi}(k,x,t)\, \mathrm{d}\,k \; ,$$

$$\tilde{\Theta}(k,x,t) = \frac{1}{\sqrt{2\pi}} \int_{-\infty}^{\infty} e^{-\mathrm{i}\,k\,z}\, \Theta(x,z,t)\, \mathrm{d}\,z \; ,$$

$$\Theta(x,z,t) = \frac{1}{\sqrt{2\pi}} \int_{-\infty}^{\infty} e^{\mathrm{i}\,k\,z}\, \tilde{\Theta}(k,z,t)\, \mathrm{d}\,k \; , \tag{9.46}$$

where the dependence on t of $\tilde{\Pi}$ and $\tilde{\Theta}$ is factored out through exponential terms, namely

$$\tilde{\Pi} = f(x)\, \mathrm{e}^{\lambda(k)\,t} \; , \qquad \tilde{\Theta} = h(x)\, \mathrm{e}^{\lambda(k)\,t} \; . \tag{9.47}$$

By employing Eqs. (9.46) and (9.47), the Fourier transformed Eqs. (9.43) and (9.45) yield

$$\left(\frac{\mathrm{d}^2}{\mathrm{d}\,x^2} - k^2 \right) f - \mathrm{i}\,k\,R\,h = 0 \; ,$$

$$\left[\frac{\mathrm{d}^2}{\mathrm{d}\,x^2} - k^2 - \sigma\,\lambda(k) - \mathrm{i}\,k\,(Pe - R\,x) \right] h - \frac{\mathrm{d}\,f}{\mathrm{d}\,x} = 0 \; ,$$

$$x = \pm\frac{1}{2} \; : \qquad f = 0 \; , \quad h = 0 \; . \tag{9.48}$$

According to the usual procedure, we define the parameter

$$\gamma(k) = \sigma\,\lambda(k) + \mathrm{i}\,k\,Pe \; , \tag{9.49}$$

so that Eq. (9.48) is rewritten as

$$\left(\frac{\mathrm{d}^2}{\mathrm{d}\,x^2} - k^2\right) f - \mathrm{i}\,k\,R\,h = 0\,,$$

$$\left[\frac{\mathrm{d}^2}{\mathrm{d}\,x^2} - k^2 - \gamma(k) + \mathrm{i}\,k\,R\,x\right] h - \frac{\mathrm{d}\,f}{\mathrm{d}\,x} = 0\,,$$

$$x = \pm\frac{1}{2} \;:\quad f = 0\,,\quad h = 0\,. \tag{9.50}$$

9.2.4 Convective Instability

The study of convective instability is based on the eigenvalue problem (9.50). Where we have to set $\Re(\lambda) = 0$ in order to detect the zero growth rate modes, that is the neutrally stable Fourier modes. On account of Eq. (9.49), we have $\Re(\gamma) = 0$. Furthermore, since $\lambda = \eta - \mathrm{i}\,\omega$, we can write $\Im(\gamma) = -\sigma\,\omega + k\,Pe = -\sigma\,\omega_\mathrm{m}$, where ω_m happens to be a modified angular frequency. Hence, Eq. (9.50) reads

$$\left(\frac{\mathrm{d}^2}{\mathrm{d}\,x^2} - k^2\right) f - \mathrm{i}\,k\,R\,h = 0\,,$$

$$\left(\frac{\mathrm{d}^2}{\mathrm{d}\,x^2} - k^2 + \mathrm{i}\,\sigma\,\omega_\mathrm{m} + \mathrm{i}\,k\,R\,x\right) h - \frac{\mathrm{d}\,f}{\mathrm{d}\,x} = 0\,,$$

$$x = \pm\frac{1}{2} \;:\quad f = 0\,,\quad h = 0\,. \tag{9.51}$$

Evidently, $\omega_\mathrm{m} = \omega$ when the forced flow is switched off, i.e. when $Pe = 0$. When $Pe \neq 0$, the forced flow has no explicit influence on the mathematical solution of the eigenvalue problem (9.51) consistently with the $(k, R, \omega_\mathrm{m})$ parametrisation. This means that, if we solve Eq. (9.51) by setting k as input parameter, we can determine numerically the eigenvalue pair (R, ω_m), independently of the Péclet number. This is the reason why the convective instability analysis is influenced by the value of Pe only when it comes to the determination of ω from ω_m. On the other hand, the neutral stability curve in the (k, R) plane is just the same as that drawn for the special case $Pe = 0$, discussed by Barletta [1].

The numerical method described in Chap. 10 is employed to solve the eigenvalue problem (9.51) and thus to obtain the neutral stability function $R(k)$. The additional difficulty with respect to the case discussed in Sect. 9.1 is that, in this case, we do not have a formal proof regarding the principle of exchange of stabilities. In other words, we cannot prove rigorously that $\Im(\gamma) = -\sigma\,\omega_\mathrm{m} = 0$. In fact, this result comes out only through the output data of the numerical solution. The neutrally stable modes for any given k happen to display a zero modified angular frequency. This inductive origin of the result $\Im(\gamma) = -\sigma\,\omega_\mathrm{m} = 0$ implies a complication in the numerical

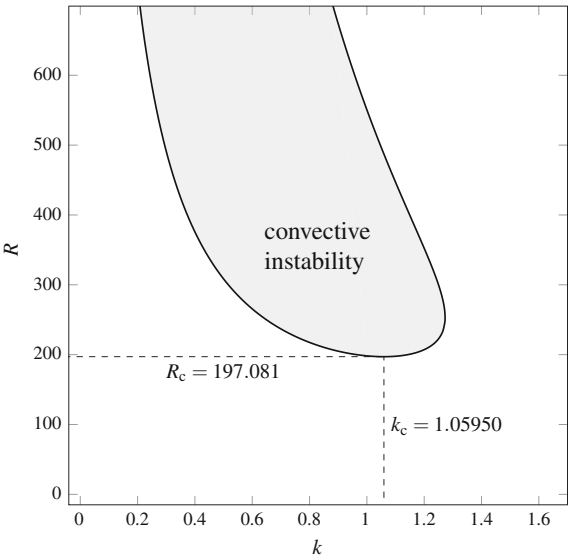

Fig. 9.8 Neutral stability curve for the vertical porous channel with isothermal and permeable boundaries

solution as we have to manage complex-valued eigenfunctions (f, h) and, hence, an effective doubled order for the differential eigenvalue problem to tackle. We have indeed to deal with a fourfold eigenfunction structure, $(\Re(f), \Im(f), \Re(h), \Im(h))$. This means a computationally heavier object to be treated numerically, but no effective difference in the algorithmic framework of the method.

Figure 9.8 displays the neutral stability curve and the convective instability region in the (k, R) plane. The shape of the curve is quite dissimilar from all that we encountered so far in the analysis of instability induced by heating from below. The neutral stability curve is not the plot of a single-valued function $R(k)$, as it happens for the Rayleigh–Bénard problem or the Horton–Rogers–Lapwood problem in their manifold variants. The neutral stability curve for the flow in a vertical porous channel has a droplike shape confining an internal region of convective instability. The point of minimum R along this curve defines the critical values k_c and R_c,

$$k_c = 1.05950\ , \qquad R_c = 197.081\ . \tag{9.52}$$

Another peculiar point along the neutral stability curve is that of maximum k, where

$$k_{max} = 1.27291\ , \qquad R_{max} = 253.340\ . \tag{9.53}$$

There was no such maximum wavelength in all our previous examples of convective instability. Its physical meaning is that Fourier modes with a wave number exceeding the maximum do not contribute to the onset of convective instability. In other terms, such large wavelength modes are ineffective in exciting an unstable response from the flow system. We mention that the numerical data used to draw the neutral

stability curve in Fig. 9.8 displayed values of σ $|\omega_{\mathrm{m}}|$ smaller than 10^{-10}. This provides inductive evidence that ω_{m} is effectively zero or, equivalently, that the relation

$$\omega = \frac{k\,Pe}{\sigma} \tag{9.54}$$

holds true for neutrally stable modes.

9.2.5 *Absolute Instability*

We now focus our analysis on the collective evolution at large times of perturbation wave packets, so that we aim to detect a possible transition from convective to absolute instability in the supercritical domain $R \geqslant R_{\mathrm{c}}$. As usual, the tool adopted to accomplish this task is the steepest-descent approximation of wave packet disturbances. This means starting from Eq. (9.48) in order to implement the saddle point condition $\lambda'(k) = 0$, with $k \in \mathbb{C}$. As in Sect. 9.1.3, we define

$$\hat{f} = \frac{\partial f}{\partial k}\,, \qquad \hat{h} = \frac{\partial h}{\partial k}\,, \tag{9.55}$$

so that the eigenvalue problem (9.48) doubles its differential order through a derivation of the differential equations and boundary conditions with respect to k, namely

$$\left(\frac{\mathrm{d}^2}{\mathrm{d}\,x^2} - k^2\right) f - \mathrm{i}\,k\,R\,h = 0\,,$$

$$\left[\frac{\mathrm{d}^2}{\mathrm{d}\,x^2} - k^2 - \sigma\,\lambda(k) - \mathrm{i}\,k\,(Pe - R\,x)\right] h - \frac{\mathrm{d}\,f}{\mathrm{d}\,x} = 0\,,$$

$$\left(\frac{\mathrm{d}^2}{\mathrm{d}\,x^2} - k^2\right) \hat{f} - \mathrm{i}\,k\,R\,\hat{h} - 2\,k\,f - \mathrm{i}\,R\,h = 0\,,$$

$$\left[\frac{\mathrm{d}^2}{\mathrm{d}\,x^2} - k^2 - \sigma\,\lambda(k) - \mathrm{i}\,k\,(Pe - R\,x)\right] \hat{h} - \frac{\mathrm{d}\,\hat{f}}{\mathrm{d}\,x} - [2\,k + \mathrm{i}\,(Pe - R\,x)]\,h = 0\,,$$

$$x = \pm\frac{1}{2}\ : \qquad f = 0\,, \quad h = 0\,, \quad \hat{f} = 0\,, \quad \hat{h} = 0\,, \tag{9.56}$$

where the condition $\lambda'(k) = 0$ has been taken into account.

The solution of the eigenvalue problem (9.56) is tackled by fixing as input data the values of Pe and $\Re(\sigma\,\lambda)$. In particular, in order to detect the threshold to absolute instability, we set $\Re(\sigma\,\lambda) = 0$. The output eigenvalues sought with the numerical

solution are $(k, R, \Im(\sigma\,\lambda))$. To this end, we employ the shooting method along the same lines discussed in Sect. 9.1.3.

There is a symmetry of the stability eigenvalue problem (9.48) which governs both the onset of convective instability and the transition to absolute instability. In fact, Eq. (9.48) is invariant under the transformation

$$x \to -x\,, \quad k \to -k\,, \quad R \to R\,, \quad Pe \to -Pe\,,$$
$$\lambda \to \lambda\,, \quad f \to -f\,, \quad h \to h\,. \tag{9.57}$$

The symmetry expressed by Eq. (9.57) ensures that the analysis of instability with a negative Péclet effectively means a reversed sign of k, but it does not imply any modification of the threshold values of R either for convective or absolute instability. This is physically not as obvious as for the instability in a horizontal layer. In fact, in the case of a vertical layer, the direction of the propagating disturbances is the vertical z-direction, where the positive or negative z-directions mean parallel or antiparallel directions with respect to gravity.

Further insights into the structure of the eigenvalue problem can be gathered by writing the complex conjugate of Eq. (9.48), namely

$$\left(\frac{\mathrm{d}^2}{\mathrm{d}\,x^2} - \bar{k}^2\right)\bar{f} + \mathrm{i}\,\bar{k}\,R\,\bar{h} = 0\,,$$
$$\left[\frac{\mathrm{d}^2}{\mathrm{d}\,x^2} - \bar{k}^2 - \sigma\,\bar{\lambda} + \mathrm{i}\,\bar{k}\,(Pe - R\,x)\right]\bar{h} - \frac{\mathrm{d}\,\bar{f}}{\mathrm{d}\,x} = 0\,,$$
$$x = \pm\frac{1}{2}\;: \qquad \bar{f} = 0\,, \quad \bar{h} = 0\,, \tag{9.58}$$

where, having in mind the transition to absolute instability, we allowed $k \in \mathbb{C}$. Both Eqs. (9.48) and (9.58) can be equivalently employed for detecting the relevant saddle points. The two eigenvalue problems coincide when we apply the transformation

$$k \to -\bar{k}\,, \quad \lambda \to \bar{\lambda}\,. \tag{9.59}$$

As a consequence, for every prescribed Pe and R, there is a pair of twin saddle points with opposite real parts and equal imaginary parts. Therefore, the values of λ for these twin saddle points have equal real parts and opposite imaginary parts. We reckon that just the same property of the pertinent saddle points for the threshold to absolute instability is implicitly reported in Figs. 9.1 and 9.2, relative to a different example. The existence of twin saddle points with opposite real parts is also displayed in Figs. 8.2 and 8.9. This situation suggests a general feature of the absolute instability analyses, even if a formal proof would require a characterisation of what a stability

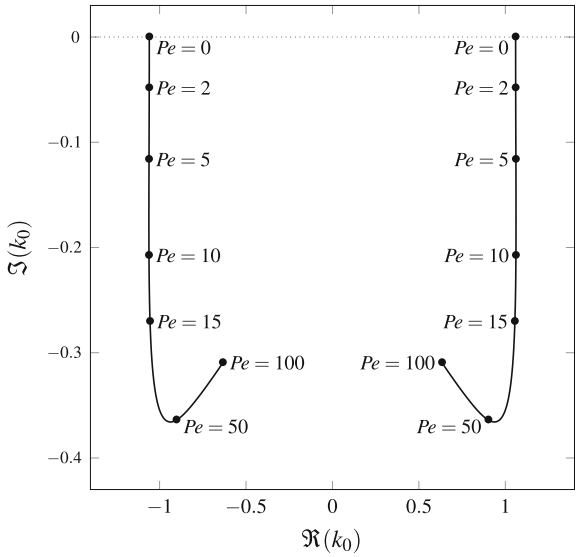

Fig. 9.9 Vertical porous channel with isothermal and permeable boundaries: migration of the pertinent saddle points, with increasing values of Pe, for the threshold to absolute instability

eigenvalue problem is meant to be. We do not aim to solve this formal conundrum here, and we focus again on our specific analysis.

On account of the above-mentioned mathematical properties of the stability eigenvalue problem, with no loss of generality, we will refer our forthcoming analysis to the case $Pe \geqslant 0$. The idea behind the search of the relevant saddle points for the transition to absolute instability is starting from $Pe = 0$ and then gradually increasing Pe. In fact, the case of no net average flow across the channel is one where we already ascertained, although inductively, that the principle of exchange of stabilities holds at neutral stability. Then, the condition of neutral stability is one where $\lambda(k) = 0$, so that we expect $R_a = R_c = 197.081$ and

$$\Re(k_0) = \pm k_c = \pm 1.05950 \,, \quad \Im(k_0) = 0 \,, \quad \Im(\sigma\,\lambda(k_0)) = 0 \,. \tag{9.60}$$

Starting from these data relative to $Pe = 0$, one can track the solution of Eq. (9.56) by gradually increasing Pe above 0. Figure 9.9 shows the migration of the twin saddle points with $Pe > 0$ originated from those given by Eq. (9.60). Figure 9.10 displays the threshold Darcy–Rayleigh number for the transition to absolute instability, R_a, plotted versus Pe and compared with the critical value $R_c = 197.081$. Once more, we see an ever- increasing gap $R_a - R_c$ as Pe increases. Furthermore, Fig. 9.11 displays the trend of $\Im(\sigma\,\lambda(k_0))$ versus Pe. Both Figs. 9.10 and 9.11 reveal some significant similarities with Figs. 9.4 and 9.2, respectively. However, there is an evident difference. The asymptotic regime for $Pe \gg 1$ where both R_a and $\Im(\sigma\,\lambda(k_0))$ are linear functions of Pe, widely discussed in Sect. 9.1.3, turns out to be unsuited to the plots reported in Figs. 9.10 and 9.11.

Another element of discrepancy emerges from Fig. 9.9. This figure appears to be dissimilar from Fig. 9.1 because there is no clue of k_0 attaining an asymptotic

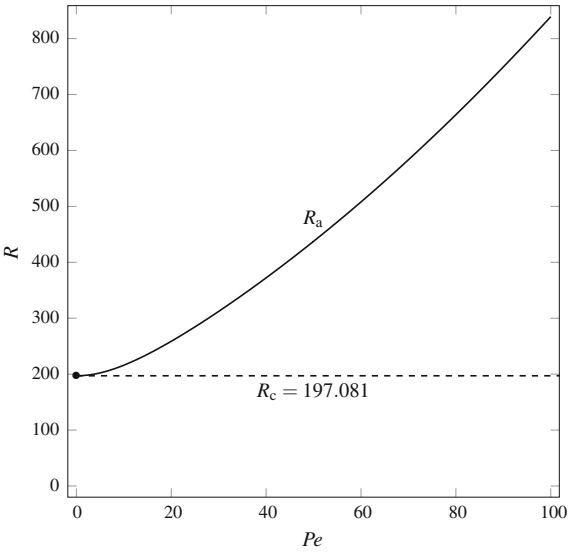

Fig. 9.10 Vertical porous channel with isothermal and permeable boundaries: plot of R_a (solid line) versus Pe, as compared with R_c (dashed line) which is independent of Pe

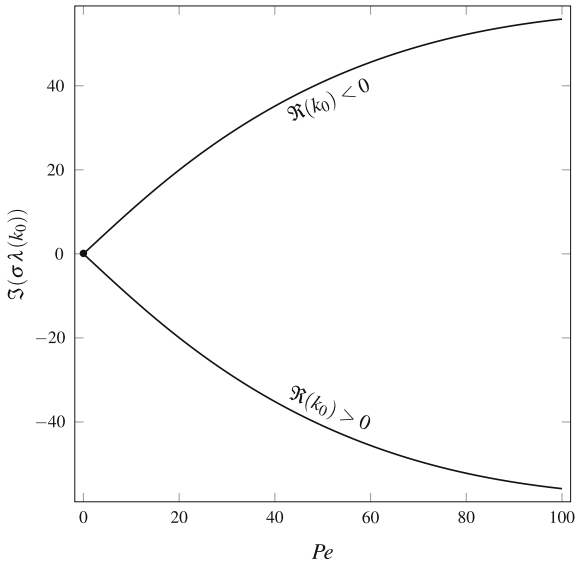

Fig. 9.11 Vertical porous channel with isothermal and permeable boundaries: plot of $\Im(\sigma\,\lambda(k_0))$ versus Pe for the saddle points k_0, at the threshold to absolute instability, with positive or negative $\Re(k_0)$

value for $Pe \to \infty$, despite the very wide range of values of Pe. In fact, we note that $Pe = 100$ is a very large value given that we are dealing with seepage flows in porous media.

An example where the fulfilment of the holomorphy requirement is satisfied is displayed in Fig. 9.12. In this figure, the test case where $Pe = 20$ and $R = R_a = 258.755$. This case corresponds to the threshold to absolute instability. The steepest-

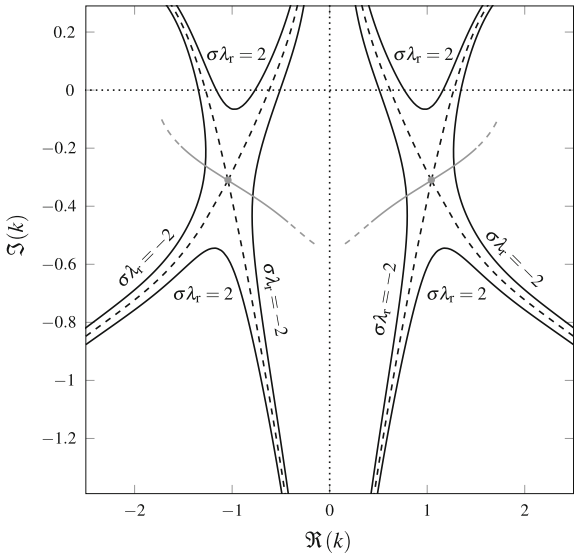

Fig. 9.12 Vertical porous channel with isothermal and permeable boundaries: map of the isolines of $\Re(\lambda) = \lambda_r$ (black solid lines) for $Pe = 20$ and $R = R_a = 258.755$. The dashed black lines are for $\lambda_r = 0$. The grey dots are the saddle points, while the grey lines are the lines of steepest descent

descent paths crossing the twin saddle points,

$$\Re(k_0) = \pm 1.04255\ , \quad \Im(k_0) = -0.311223\ ,$$

$$\Im(\sigma\,\lambda(k_0)) = \mp 19.9514\ , \tag{9.61}$$

are drawn as grey lines. It is evident from Fig. 9.12 that no singularities appear within the region of the k plane around the saddle points. Thus, one can devise a continuous deformation of the real axis, $\Im(k) = 0$, matching locally the steepest-descent paths. In other words, the holomorphy requirement can be considered as satisfied. Just the same conclusions can be drawn by considering Fig. 9.13 relative to the case where $Pe = 50$ and $R = R_a = 437.549$. Again, we are considering a threshold value of R for the onset of absolute instability, with the pertinent saddle points being, in this case,

$$\Re(k_0) = \pm 0.902055\ , \quad \Im(k_0) = -0.363949\ ,$$

$$\Im(\sigma\,\lambda(k_0)) = \mp 40.9155\ . \tag{9.62}$$

Such saddle points are denoted as grey dots in Fig. 9.13. We conclude that, in both the test cases examined in Figs. 9.12 and 9.13, the holomorphy requirement is satisfied.

We recall from Definition 4.2 and Eq. (4.50) that the transition to absolute instability is mathematically associated with a transition from a negative to a positive $\Re(\lambda(k_0))$. In fact, the numerical solution of Eq. (9.56) can be carried out, not only by setting $\Re(\lambda) = 0$, but also by prescribing any negative or positive value of $\Re(\lambda)$. This alternative serves to evaluate R versus Pe corresponding to negative or positive

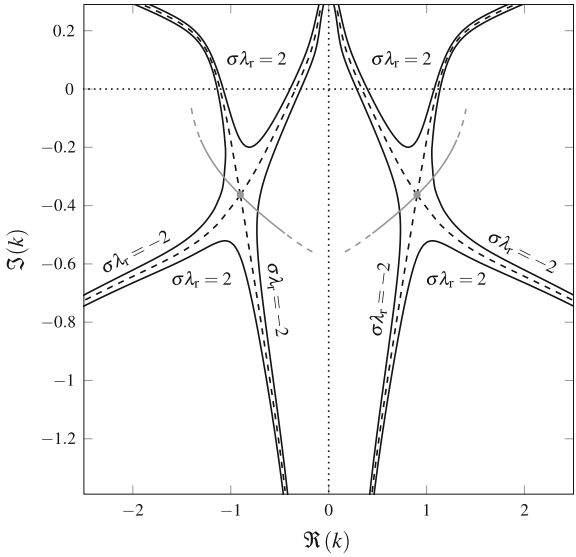

Fig. 9.13 Vertical porous channel with isothermal and permeable boundaries: map of the isolines of $\Re(\lambda) = \lambda_r$ (black solid lines) for $Pe = 50$ and $R = R_a = 437.549$. The dashed black lines are for $\lambda_r = 0$. The grey dots are the saddle points, while the grey lines are the lines of steepest descent

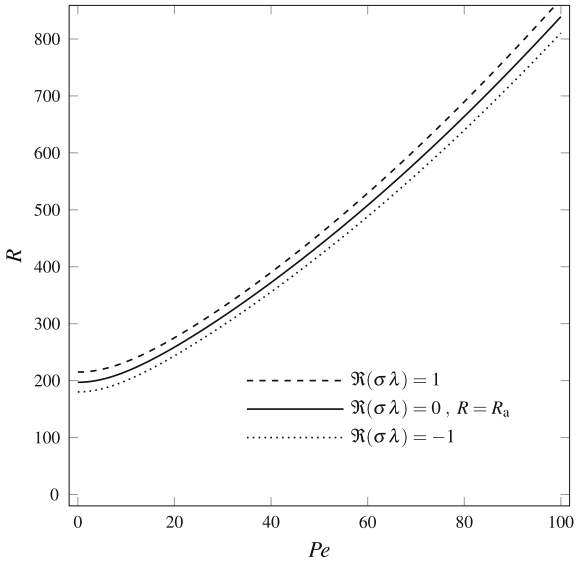

Fig. 9.14 Vertical porous channel with isothermal and permeable boundaries: plot of R_a (solid line) versus Pe, as compared with R versus Pe evaluated for negative and positive growth rates $\Re(\lambda)$ (dotted and dashed lines)

growth rates of the wave packet disturbances. The result is reported in Fig. 9.14 where the solid line showing the trend of R_a versus Pe is displayed together with the dotted line relative to an absolutely stable condition, $\Re(\sigma\,\lambda) = -1$, and the dashed line relative to an absolutely unstable condition, $\Re(\sigma\,\lambda) = 1$. As expected, these plots show that the absolutely unstable case, $\Re(\sigma\,\lambda) = 1$, corresponds to values of R larger than R_a, while the opposite occurs for the absolutely stable case, $\Re(\sigma\,\lambda) = -1$.

9.3 Concluding Remarks Regarding Numerical Solutions

We have seen the numerical method applied to the solution of absolute stability problems. One would have expected some intrinsic extra difficulty emerging when an analytical dispersion relation is not available or when it is too complicated to be practically preferable with respect to a numerical solution. In fact, the treatment of a numerical instance of absolute instability involves the solution of an ordinary differential eigenvalue problem. The order of such eigenvalue problem is doubled if compared with that involved in establishing the convective instability threshold. Moreover, the absolute instability eigenvalue problem involves complex eigenfunctions even if the neutral stability condition requires only real eigenfunctions. However, the algorithm for the numerical solution is not different from that employed for the convective instability analysis. Another important element is that, even when an analytical dispersion relation is available and it is expressed with simple rational functions, as it happens for the Prats problem discussed in Sect. 8.2, the evaluation of the saddle points needs the use of a numerical root-finding procedure. At least, this is what happens in general except for some very special cases. These considerations suggest that some numerical computation within the absolute instability analysis emerges in every case, even when the stability dispersion relation is expressed analytically. Our conclusion is that there is no true additional encumbrance, or limitation in the amount of results that can be gathered, when the stability analysis is to be carried out in a fully numerical framework.

References

1. Barletta A (2015) A proof that convection in a porous vertical slab may be unstable. J Fluid Mech 770:273–288
2. Dongarra JJ, Straughan B, Walker DW (1996) Chebyshev tau-QZ algorithm methods for calculating spectra of hydrodynamic stability problems. Appl Numer Math 22:399–434
3. Gill AE (1969) A proof that convection in a porous vertical slab is stable. J Fluid Mech 35:545–547
4. Prats M (1966) The effect of horizontal fluid flow on thermally induced convection currents in porous mediums. J Geophys Res 71:4835–4838
5. Straughan B, Walker DW (1996) Two very accurate and efficient methods for computing eigenvalues and eigenfunctions in porous convection problems. J Comput Phys 127:128–141